Fuel 352 (2023) 129045

Contents lists available at ScienceDirect

Fuel

journal homepage: www.elsevier.com/locate/fuel

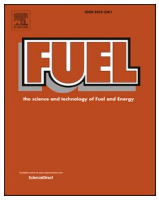

Full Length Article

Catalytic production of γ-valerolactone, a biofuel precursor, from furfural in one-pot: Synergistic effect between Zr and Sn

Adrián García [a], Rita Sánchez-Tovar [a], Pablo J. Miguel [a], Elena Montejano-Nares [b], Francisco Ivars-Barceló [b], Juan Antonio Cecilia [c], Benjamín Torres-Olea [c], Benjamín Solsona [a,*]

[a] Dept. Chemical Engineering, Universitat de València. Av. Universitat s/n, 46100 Burjassot, Valencia, Spain
[b] Dept. Química Inorgánica y Química Técnica, Facultad de Ciencias, UNED, Av. Esparta s/n, Las Rozas, 28232 Madrid, Spain
[c] Dept. Química Inorgánica, Cristalografía y Mineralogía, Campus de Ciencias, Universidad de Málaga, 29071 Málaga, Spain

ARTICLE INFO

Keywords:
Synergistic effect
Sn
Zr
Zeolite
Furfural
γ-Valerolactone
Biomass derived substrates: One pot

ABSTRACT

This work presents for the first time the synergistic effect of tin and zirconium for the one pot transformation of furfural into γ-valerolactone. Furfural is a versatile product that can be easily produced from lignocellulosic biomass and can be transformed into valuable products such as γ-valerolactone, which can be used to produce different types of chemicals, fuels and as a green solvent. The transformation of furfural into γ-valerolactone in one-pot has been studied using Sn and Zr based catalysts supported on treated zeolite Y. These catalysts were characterized by N_2 adsorption, IR, UV–vis, XRD, TEM, pyridine adsorption-IR and XPS in order to determine their physicochemical properties. For all the studied compositions, mixed bimetallic Sn-Zr catalysts led to higher γ-valerolactone yields than those monometallic Sn or Zr catalysts. The bimetallic catalyst with a Sn:Zr at. ratio of 1:1 achieved the best performance, reaching a yield to γ-valerolactone of ca. 80 % after only 1 h of reaction at 180 °C using 2-propanol as a hydrogen source. The best performance of the bimetallic catalyst has been related to the broad dispersion of the metals on the surface of the support, forming mixed dispersed Zr-O-Sn surface species, favoring an adequate amount of Lewis and Brønsted acid sites. Moreover, for this catalyst, stability was very high, showing constant yield values to γ-valerolactone after at least 4 uses, which can be related to the high and stable interaction between the surface metal species and the support.

1. Introduction

The consumption of fossil fuels and the demand for chemicals have significantly increased in the recent years due to technological development and current needs. Population continues increasing and it is foreseen to reach 9 billion by 2050. Thus, the energy consumption is expected to increase even more [1]. However, fossil fuels are non-renewable, thus it is necessary to find alternative energy sources. Furthermore, fossil fuels produce greenhouse gases, especially CO_2, which is the primary greenhouse gas emitted through human activities. An increase in CO_2 concentration in the atmosphere is directly related to global warming and climate change [2]. In the last decades, new renewable energy sources such as wind, solar, geothermal, nuclear, hydroelectricity and biomass [3] have been studied in order to substitute fossil fuels. Among them, lignocellulosic biomass might be used as an alternative energy source to replace crude oil, as biorefineries are not only a source of chemicals and fuels but also energy [4,5]. However, this technology is not fully developed since every year tons of biomass are burnt or sent to landfills [6,7].

Lignocellulosic biomass can be treated and decomposed in its main biopolymers: cellulose (30–50 %), hemicellulose (20–35 %) and lignine (15–20 %) [8]. Cellulose and hemicellulose are formed by five and six carbon sugars, mainly xylose, arabinose, galactose, mannose, glucose and glucuronic acid. However, lignine is a complex polymer made by cross-linking phenolic precursors [9,10].

From cellulose and hemicellulose, glucose, arabinose or xylose can be easily produced through a dehydration reaction [11,12]. These sugars can be transformed into building block molecules including 5-hydroxymethylfurfural (HMF), furfural (FF), lactic acid, sorbitol, levulinic acid (LA), formic acid (FA) and γ-valerolactone (GVL) [13–18].

One of the most important building blocks is GVL, which can be used as a renewable carbon source for the production of chemicals, fuels and as a green solvent [19]. GVL has a very low toxicity, high boiling point (207 °C), high flash point (96.1 °C) and a low melting point (-31 °C)

* Corresponding author.
E-mail address: benjamin.solsona@uv.es (B. Solsona).

https://doi.org/10.1016/j.fuel.2023.129045
Received 31 March 2023; Received in revised form 8 May 2023; Accepted 16 June 2023
Available online 21 June 2023

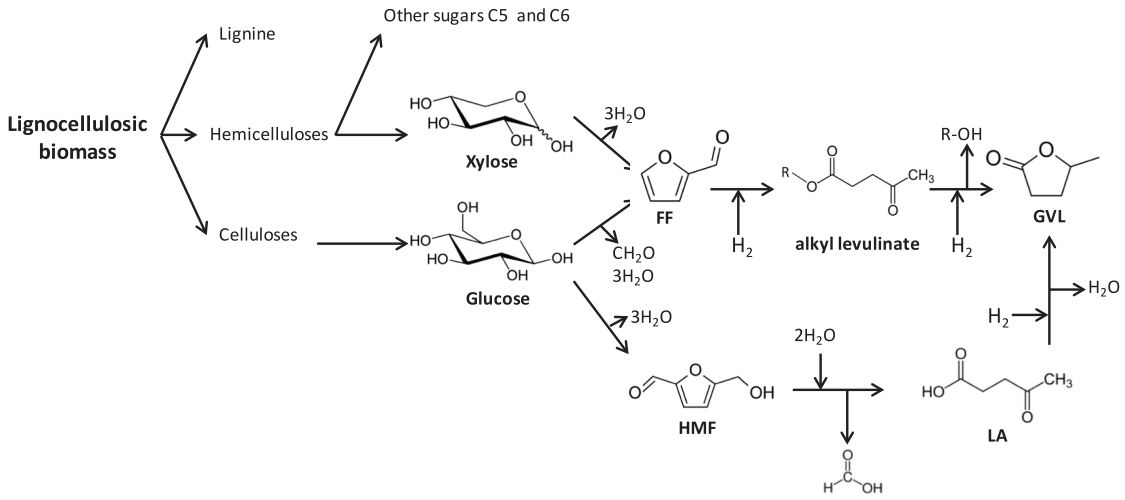

Fig. 1. Production of furfural from lignocellulosic biomass.

[20–22]. GVL can be produced from derived biomass compounds by hydrogenation. Many hydrogen sources were studied to carry out the hydrogenation reaction such as molecular hydrogen, formic acid (FA) and alcohols [22,23]. In the reduction of FF, alcohols have been used as a hydrogen donors to reduce aldehyde or ketones to the corresponding alcohols through Meerwein-Ponndorf-Verley (MPV), forming the homologous aldehyde or ketone after the hydrogenation of primary or secondary alcohol, respectively [19,24]. Many studies have been focused on the use of LA and their respective esters to produce GVL using alcohols as H-donor by catalytic transfer hydrogenation (CTH) through MPV route because the reaction process is well known and easier than with other intermediates compounds [14,25–28]. Interestingly, several studies have been conducted using FF as a substrate, another intermediate compound that can be easily produced by dehydration of xylose [29–32].

On the other hand, furfural is an aromatic aldehyde with a ring structure of 5 carbons. FF can be used for different applications such as solvents, monomers and pharmaceuticals but also as a suitable platform chemical [33–35]. FF can be produced by dehydration of C5 sugars via the acid hydrolysis of lignocellulosic biomass [30,36] (Fig. 1). Moreover, some studies showed that FF can be produced from hemicelullose or directly from crops, such as corn stalk, using solid catalysts [18,37–39].

The production of GVL from FF can occur by cascade reactions. A combined catalyst system containing both Lewis (LAS) and Brønsted acid sites (BAS) produces the FF transformation into GVL in one-pot cascade process [40–44]. The most studied heterogeneous catalysts are based on Zr, as the Lewis acid generator to catalyze the MPV hydrogen transfer reactions, and aluminum-containing acid zeolites (H-Beta, H-ZSM-5 or H-Y), which present Brønsted acid sites [45–49]. Since both types of acid sites are required to transform FF into GVL in one-pot, a suitable mixture of them is essential to optimize the GVL production [50–52].

For example, Bui et al. designed a catalytic system of a Lewis acid Zr-Beta and a Brønsted acid Al-MFI zeolite to transform FF into GVL. Then, a yield to GVL of 78 % was achieved using 2-butanol after 48 h at 120 °C [53]. A similar study was carried out by Zhang et al., where a catalytic system of Zr supported on dealuminated zeolite Y and zeolite Y in 2-pentanol was designed [47].

Interestingly, catalytic systems in which apparently Brønsted acid sites are not present in the bare support (for instance, siliceous supports), can also generate reasonable yields to GVL. This is probably due to the generation of those Brønsted sites when Zr is added to the catalyst. Then, the formation of Brønsted acid sites in Zr on silica may take place due to a high Lewis acid sites density interacting with surface –OH groups [43,54,55]. A yield to GVL of 37 % was achieved by Iglesias et al., using Zr supported on silica and 2-propanol, after 7 h of reaction at 170 °C [55]. A yield to GVL of 80 % was obtained in another study using Zr supported on siliceous spheres [43].

Although less studied, Sn-containing catalysts can also transform FF into GVL since the presence of Sn^{4+}-species can also promote the presence of Lewis acid sites [45,56]. However, there is no work in the literature studying the catalytic reaction to produce GVL from FF using bimetallic catalysts containing both Sn and Zr. Therefore, the aim of this work is to evaluate a possible synergistic effect that Sn and Zr-species might have in the formation of Lewis and Brønsted acid sites.

Thus, in the present work, a bimetallic catalyst of Sn and Zr supported on dealuminated Y zeolite was optimized in order to produce GVL from FF in one-pot using 2-propanol as a solvent and H-donor. It will be shown, for the first time, that a clear synergistic effect between Sn and Zr sites takes place allowing high yields to γ-valerolactone, higher than that achieved by catalysts with only Zr or only Sn. The best catalyst was selected to study the transformation of other biomass derived substrates into GVL.

2. Materials and methods

2.1. Reagents

The synthesis of Zr-Sn doped zeolite Y was carried out using zirconium (IV) oxynitrate hydrate ($ZrO(NO_3)_2{\cdot}xH_2O$ (99 % purity) from Sigma-Aldrich, St. Louis, MO, USA), tin (II) oxalate (SnC_2O_4 (98 % purity) from Sigma-Aldrich, St. Louis, MO, USA), zeolite Y Si/Al = 15 (100 % purity from Zeolyst International, Conshohocken, PA, USA), nitric acid (HNO_3 puriss. p.a. ≥ 65%, from Sigma-Aldrich, St. Louis, MO, USA), oxalic acid ($H_2C_2O_4{\cdot}2H_2O$, purity 99.5 %, ACROS Organics). For the reaction furfural (99 % purity), ethyl levulinate (99 % purity), methyl levulinate (98 % purity), levulinic acid (98 % purity), 2-propanol (99.5 % purity) from Sigma-Aldrich, St. Louis, MO, USA were used.

2.2. Preparation of catalysts

Zeolite Y (Al-HY) with a Si/Al = 15 at. ratio was dealuminated with HNO_3 in an aqueous solution (a mixture of 18.4 mL of water and 21.6 mL of HNO_3 per 2 g of zeolite) at 80 °C for 24 h. Afterwards, the mixture was cooled, centrifugated to recover the zeolite and washed with deionized water to remove the nitric acid. The dealuminated zeolite was dried in a furnance at 100 °C overnight. The dealuminated zeolite was labelled as HY. The delumination process led to a sample with a poor Al loading (Si/Al = 85 at. ratio).

Table 1
Physico-chemical characteristics of the Zr and Sn based catalysts.

Catalyst	Sn:Zr at. ratio[a]	Chemical analysis [b]		Surface area (m^2/g)	V_a (cm^3/g)[c]	D_p (Å)[d]	Crystallite size SnO_2[e]	Crystallite size ZrO_2[e]
		Sn/Si	Zr/Si					
HY	–	0	0	998.8	0.48	60.4	–	–
SnO_2	∞	∞	–	22.3	0.06	228.6	14.2	–
Sn/Y	∞	0.18	0	715.2	0.37	62.2	10.0	–
SnZr/Y(9:1)	9:1	0.16	0.021	703.5	0.35	62.1	9.4	n.d
SnZr/Y(1:1)	1:1	0.08	0.08	730.0	0.34	60.7	n.d	n.d
SnZr/Y(1:9)	1:9	0.020	0.17	774.4	0.39	61.0	n.d	5.6
Zr/Y	0	0	0.19	802.0	0.39	60.2	–	6.2
ZrO_2	0	–	∞	59.0	0.14	85.1	–	9.0

[a] Sn:Zr at. ratio in the synthesis (theoretical).
[b] Sn/Si or Zr/Si in at. ratio (determined by ICP).
[c] Single point adsorption total pore volume of pores less than 354.944 Å width at $P/P_0 = 0.94$.
[d] BJH Desorption average pore width.
[e] Determined by XRD (Scherrer equation).

Zr- and Sn-species were incorporated by a wet impregnation method using deionized water as solvent. The calculated content of the metal precursor ($ZrO(NO_3)_2{\cdot}xH_2O$ or/and SnC_2O_4) and oxalic acid was added into deionized water. Oxalic acid was added in a molar relation metal: oxalic acid (1:3). Then, the dealuminated zeolite was added to the mixture and it was placed into a hot plate under stirring until the solvent was totally evaporated. The metal precursor amount added was Si/metal = 5 (assuming that all dealuminated zeolite was SiO_2). Those catalysts were labelled as Sn/Y or Zr/Y. Bimetallic catalysts were synthesized using a Sn:Zr atomic ratio of 9:1; 1:1 and 1:9 and they were labelled as SnZr/Y(9:1), SnZr/Y(1:1) and SnZr/Y(1:9), respectively. Finally, samples were dried at 100 ºC for 12 h and later calcined at 500 ºC in static air for 6 h.

For comparison, samples with either Sn or Zr on the zeolite Y with the optimal loading were also prepared following the same procedure.

2.3. Characterization techniques

Power X-ray diffraction (XRD) patterns of catalysts were collected at two angles between 10 and 80 º using an Enraf Nonius FR590 sealed tube diffractometer (Bruker, Delft, The Netherlands) equipped with a monochromatic Cu Kα1 source (30 mA and 40 kV).

Diffuse reflectance ultraviolet–visible (UV–Vis) spectra were measured on a UV-2600 Shimadzu equipped with a "Praying Mantis" attachment from Harrick.

Fourier transform infrared spectroscopy (FTIR) analysis of samples was performed using a Cary 600 spectrometer (Agilent Technologies) with a resolution of 4 cm^{-1} and a scanning frequency of 32 min^{-1} at room temperature. Spectra were registered in the 4000–500 cm^{-1} region.

High resolution Transmission Electronic Microscope (HR-TEM) was used in order to analyze the catalyst structure and morphology, employing a field emission gun TECNAI G2 F20 microscope (FEI Company, Hillsboro, OR, USA) at 200 kV and a JEM 3000F microscope (JEOL, Tokyo, Japan, 300 kV). This equipment was also used for energy dispersive X-ray (EDX) and selected area electron diffraction (SAED). Firstly, a sonication treatment for 20 min was carried out in ethanol and deposited on a holey carbon film supported on a copper grid.

N_2 adsorption–desorption isotherms were acquired at −196 ºC and measured on a Micromeritics Tristar apparatus with enhanced secondary void system after outgassing at 150 ºC before reaching vacuum conditions. Surface area was determined by the Langmuir and BET method. The pore diameter was determined from the BJH method.

In order to evaluate the Lewis and Brønsted acidity analysis of pyridine adsorption was performed using a Bruker Vertex 70 instrument equipped with a Pike DiffusIR cell attachment and recorded with an MCT detector after 128scans and with a 4 cm^{-1} resolution in the region 4000–450 cm^{-1} to acquire in situ DRIFT spectra. Samples were loaded and pre-treated in a He flow (10 mL min^{-1}) for 1 h at 300 ºC. Spectra were acquired after the pretreatment at different temperatures (300, 250, 200, 150, 100 and 50 ºC). After the pretreatment the samples were exposed to pyridine vapour (1 μL) for 20 min at 50 ºC, followed by re-evacuation at 50–300 ºC and IR spectra were measured at the different temperatures (50, 100, 150, 200, 250 and 300 ºC).

X-ray photoelectron spectra (XPS) were measured at room temperature using a Mg Kα ($h\nu = 1253.6$ eV) X-ray radiation source operated at 300 W. An electrostatic hemispherical analyzer equipped with 7 channel trons was employed, which is a custom-made analyzer package refurbished by SPECS recovering an out of service Scienta Omicron hardware and combining it with SPECS HSA 3500 + electronics and SpecsLab Prodigy software. The default detector voltage was kept constant at 2000 eV for all measurements and the high-resolution spectra were acquired with pass energy of 30 eV and an energy step of 0.1 eV. The base pressure in the analysis chamber was kept below 3×10^{-8} mbar during the analyses. The calibration for the binding energy scale was carried out according to the C(1 s) peak at 484.5 eV in all cases.

Lorentzian-Gaussian line-shape backgrounds were used for the curve fittings of Sn3d and Zr3d core levels. Spectrometer transmission function, cross section, and inelastic mean free path values from CasaXPS software were employed for quantitative calculations.

2.4. Catalytic test and analysis

Furfural conversion was carried out in an autoclave reactor, which was covered by a Teflon container of 25 mL. In a typical run, 5 mL of 2-propanol, 0.25 mmol of FF and 0.2 g of catalyst were added to the reactor. Then, the reactor was purged using N_2 and sealed. It was placed in a silicon bath at the desired temperature and stirred at 800 rpm. When the reaction finished, the reactor was cooled in an ice-bath and the liquid product was recovered by filtration for the quantitative analysis.

Experiments using levulinic acid, methyl levulinate and ethyl levulinate were conducted to produce GVL. The reaction was carried out using 5 mL of 2-propanol, 0.25 mmol of substrate and 0.2 g of catalyst for 1 h at 180 ºC.

The products were analyzed by a gas chromatograph (GC), using a HP 5890 GC instrument (Hewlett Packard, Palo Alto, CA, USA). The GC has an Agilent HP-1 column (30 m × 0.32 mm × 0.25 μm) an injection port at 220 ºC and a flame ignition detector (FID) at 240 ºC. The temperature program for a typical run was as follows: (i) 35 ºC isothermal for 30 min, (ii) a heating rate of 1.5 ºC min^{-1} from 35 to 230 ºC and (iii) 230 ºC isothermal for 30 min. In order to identify other reaction by-products a gas chromatography-mass spectrometer was used (GC-MS5977A MSD-7890A, Agilent, Santa Clara, CA, USA). The temperature program used was the same as for the GC-FID.

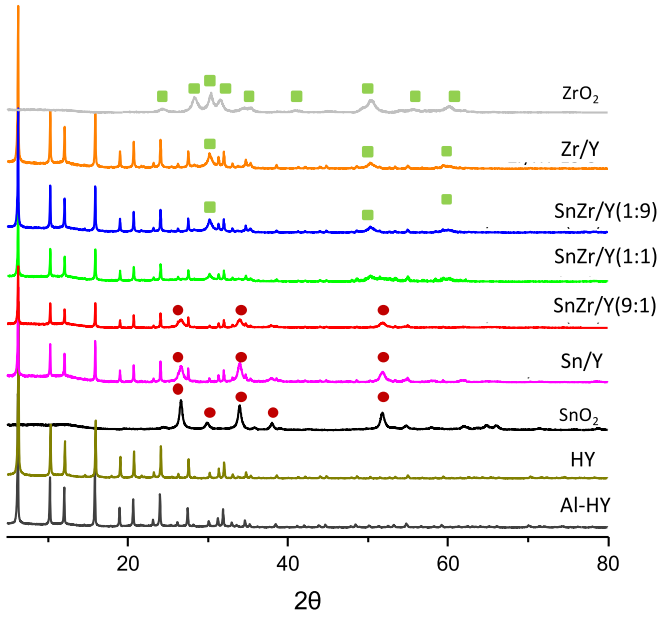

Fig. 2. XRD patterns of SnO_2, ZrO_2, HY and Al-HY and the synthesized catalysts. (●) SnO_2, (■) ZrO_2.

2.5. Recycle of catalyst

For the recycling test, the reaction was carried out with 0.5 g of catalyst and after 3 h of reaction, the solid catalyst was recovered by filtration and it was dried at 180 ºC for 12 h in order to be reused in the next cycles. For the second cycle of reaction 0.2 g of recycled catalyst were used for the reaction. The same procedure was carried out for the third cycle of reaction, i.e.; 0.2 g of recycled catalyst in the second cycle was used to perform the reaction.

3. Results and discussion

3.1. Characterization results

Some physicochemical properties of the synthesized catalysts, including the surface area, the total volume pore and the pore diameter, are shown in Table 1. The support chosen for this study is dealuminated HY zeolite since it has been reported to present adequate properties as a support such as a suitable acidity [57]. Representative characteristics of the parent zeolite and a comparison with the dealuminated zeolite are shown in Supporting Information. The addition of metals to the dealuminated zeolite leads to an expected decrease in the surface area, which is more important when Sn is added rather than with Zr. Similarly, the total pores volume (V_a) is also reduced when metal is added to the support.

Figure S1 shows the N_2 adsorption–desorption isotherms at −196 ºC for the monometallic and bimetallic catalysts with an at. Sn:Zr ratio of 1:1. The support and all the catalysts exhibited an isotherm type I due to the high N_2-adsorption at low relative pressure. These profiles are typical of materials with high and defined microporosity as zeolitic materials (Fig. S1A). On the other hand, the N_2 adsorption isotherms of pure SnO_2 and ZrO_2 presents an isotherm intermediate between type II and III, indicating low porosity and weak interaction between the adsorbate and adsorbent (Fig. S1B). The increase of the N_2-adsorption at high relative pressure suggests the presence of a material with microporosity due to the N_2-filled between adjacent particles.

The UV–vis spectra of representative catalysts are shown in Figure S2. In the case of pure SnO_2 catalysts a band centred at ca. 350 nm is clearly observed. This band is attributed to the existence of crystalline tin oxide [58]. Apart from being observed in pure SnO_2, this band can be clearly detected in the Zr-free supported Sn/Y catalyst. The same band but with lower intensity has been also observed in the bimetallic catalyst with the highest amount of Sn (SnZr/(9:1)). Additionally, a band centred at ca. 250 nm associated with dispersed Sn-Ox species interacting with the support has been observed in all the Sn-containing samples.

In the case of the Zr-related features, a band at ca. 230 nm caused by Zr-O-Zr charge transfer in bulk ZrO_2 was observed in the pure ZrO_2 sample [43,47]. In the case of Zr-supported catalysts a band located at ca. 210 nm, which is attributed to ligand-to-metal charge transfer from O^{2-} to Zr^{4+} ion in the tetrahedral configuration, was observed in the Zr/Y and SnZr/Y(1:9) catalysts [47].

These samples were also characterized by FTIR spectroscopy (Figure S3). The FTIR spectra of the the Sn and/or Zr supported catalysts do not show appreciable differences with the bare HY support, showing the typical pattern of the zeolitic material. Only representative peaks at ca. 750 cm^{-1} and 675 cm^{-1}, which are related to the stretching vibrations of Me-O bonds [59,60] have been observed in pure metallic oxides (ZrO_2 and SnO_2, respectively).

These catalysts were also characterizated by X-ray diffraction (Fig. 2). The X-ray diffractograms of the catalysts, the HY support and pure ZrO_2 and SnO_2 are shown in Fig. 2. The HY support presents a XRD pattern typical of the Y zeolite with the main peaks at 6.3, 10.3, 12, 15.9, 18.9, 20.7, 23.9, 27.4, 31.8º. The catalysts with Sn and/or Zr also present the typical diffractions of the zeolite, but with lower intensities. It is important to note that the dealumination process and subsequent metal incorporation has been reported to cause contraction and expansion, respectively, of the zeolite framework [47,61,62].

The X-ray difractogram of pure ZrO_2 indicates the presence of ZrO_2 with peaks at 2θ = 17.5, 24.1 28.1, 30.2, 31.6, 34.2, 34.6, 40.6, 50.3, 51 and 60º, which mainly correspond to ZrO_2 in its monoclinic form (JCPDS: 37–1484) with the difraction peaks at 2θ = 28.1, 31.6 and 50.3º. Moreover, typical reflexions from tetragonal ZrO_2 were also detected (JCPDS 88–1007) [63]. These peak related to crystalline ZrO_2 phase could be also detected in the supported catalysts especially in that with only Zr (Zr/Y) and that with Zr and Sn with the highest Zr-loading (SnZr/Y(1:9)).

Unsupported SnO_2 sample shows the main peaks at 2θ = 26.7, 33.9, 37.9, 51.8, 54.6 and 58.1 ° corresponding to the the (110), (101), (200), (211), (310) and (301) planes, which is in agreement with the pattern of SnO_2 [(JCPDS) 41–1445] [64]. Interestingly, peaks related to SnO_2 were also detected in the supported catalysts with high Sn-loading (Sn/Y and SnZr/Y(9:1)), indicating that bulk SnO_2 is also present in these supported catalysts.

The presence of bulk metal oxides on the catalysts could be due to an excess of metal ions over the amount of removed Al^{+3} sites from the parent zeolite. Therefore, it is likely that the extra metal (Sn or Zr) could not be accommodated in the framework vacancies. Nevertheless, in the bimetallic catalyst with the same proportion of Sn and Zr (SnZr/Y(1:1)), the presence of SnO_2 nanoparticles is not observed, suggesting either a high dispersion of SnOx or SnZrOx species on the support or the presence of very tiny SnO_2 crystallites.

The crystallite size of the metal oxides nanoparticles (ZrO_2 and SnO_2) in the catalysts, can be estimated by the Scherrer equation (Table 1). The larger crystallites were detected in the samples without support (pure SnO_2 and pure ZrO_2), especially in the case of pure SnO_2. In the catalyst of Sn supported on zeolite (Sn/Y) the crystallite diameter of SnO_2 particles decreased compared to that of pure SnO_2. This decrease was sharper in the bimetallic catalyst with a Sn:Zr at. ratio of 9:1. A similar observation (decrease if supported and if the other metal was present in the composition of the catalyst) took place regarding the ZrO_2 crystallite size. Interestingly, the crystallite size of SnO_2 and ZrO_2 could not be estimated by XRD for the catalyst with an intermediate composition SnZr/Y, since the peaks of the metal oxides were not clearly observed in the X-ray diffractograms (Fig. 2). Similarly, in the SnZr/Y(9:1) and SnZr/Y(1:9) catalysts the crystallite diameter of ZrO_2 and SnO_2, respectively, could neither be estimated.

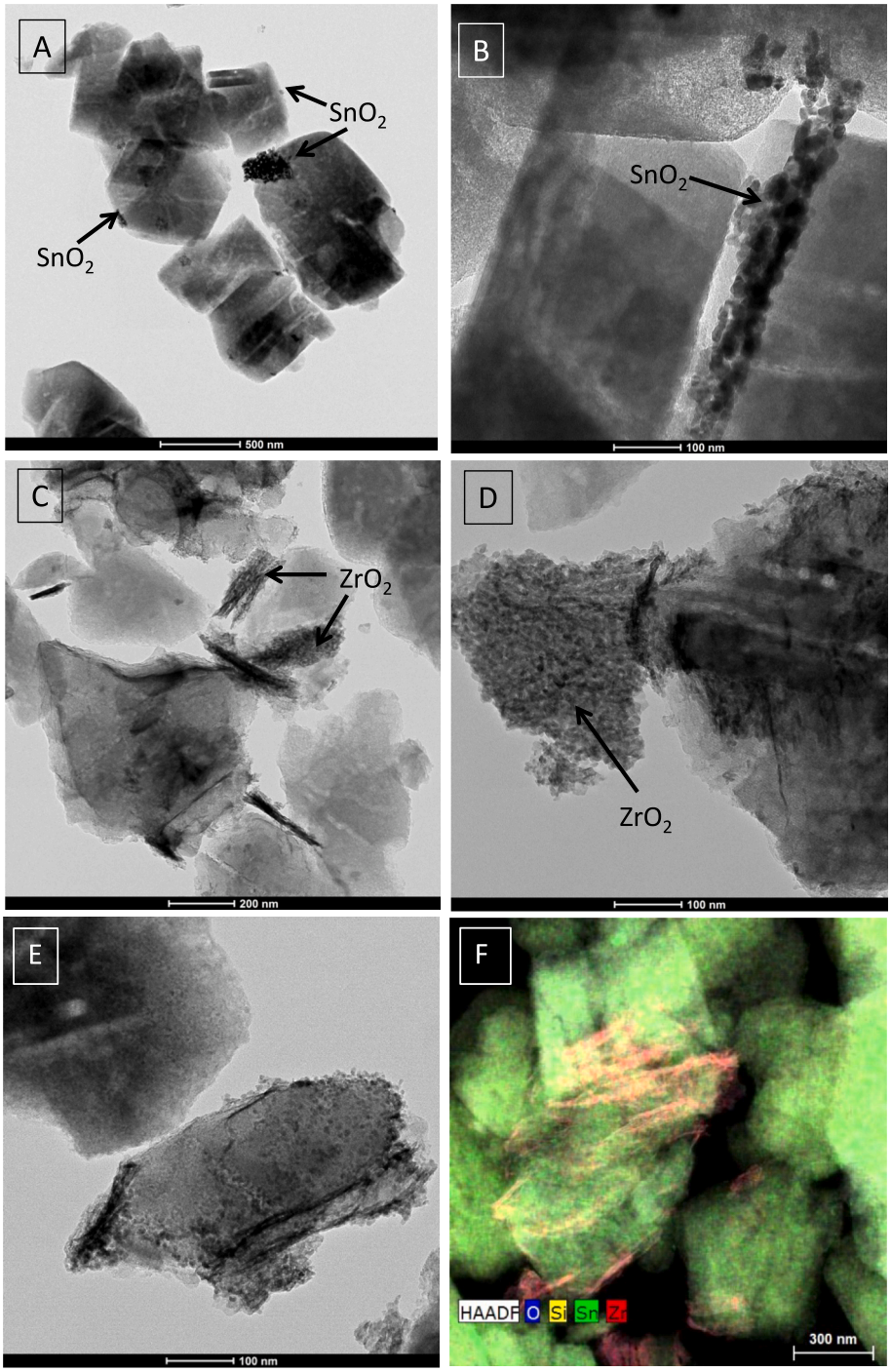

Fig. 3. TEM images of catalysts Sn/HY-15-5 (A, B), Zr/HY-15-5 (C,D) y Sn:Zr/HY-15-5-(1:1) (E, F).

As XRD only provides information of crystalline phases if the crystallite size is higher than ca. 4 nm, the catalysts were analyzed by high resolution transmission electronic microscopy (TEM). Additionally, TEM analysis also provides information about the morphology and the distribution of Sn and Zr on the support.

TEM images of the support before and after the dealuminization treatment and from pure SnO_2 and ZrO_2 compounds are shown in the Figure S4 whereas those of SnZr/Y(9:1) and SnZr/Y(1:9) catalysts can be seen in Figure S5. The zeolite does not undergo changes in its structure or morphology after the dealuminization treatment. On the other hand, pure SnO_2 forms aggregates of spherical particles with an overall cylindrical shape. Similarly, pure ZrO_2 consists of particle aggregates, although with lower size than SnO_2 particles.

Fig. 3 shows the TEM images of Zr/Y, Sn/Y and SnZr/Y(1:1) catalysts. Regarding the monometallic catalysts, it can be observed that all the metal added to the support has not been fully dispersed. In fact, aggregates of metal oxide particles were clearly observed on the support. However, in the case of the bimetallic catalyst SnZr/Y(1:1), (Fig. 3E-F), most of Sr and Zr are dispersed on the surface of the dealuminated sample and only a very low amount of aggregates of ZrO_2 particles has been observed. The mapping of this sample shows that tin was homogeneously dispersed on the surface of the zeolite without the presence of aggregates whereas Zr, being less dispersed, was always in contact with tin. On the contrary, in the bimetallic catalysts rich in Sn (SnZr/Y(9:1))

Table 2
Acidity data obtained by pyridine adsorption and BAS/LAS ratio.

Sample	Total acidity ($\mu mol_{pir}/g$)	Total acidity ($\mu mol_{pir}/m^2$)	BAS/LAS ratio
HY	231.9	0.23	0.020
Sn/Y	368.6	0.52	0.104
SnZr/Y (9:1)	805.2	1.14	0.118
SnZr/Y (1:1)	530.6	0.73	0.187
SnZr/Y (1:9)	624.9	0.81	0.032
Zr/Y	259.0	0.32	0.007

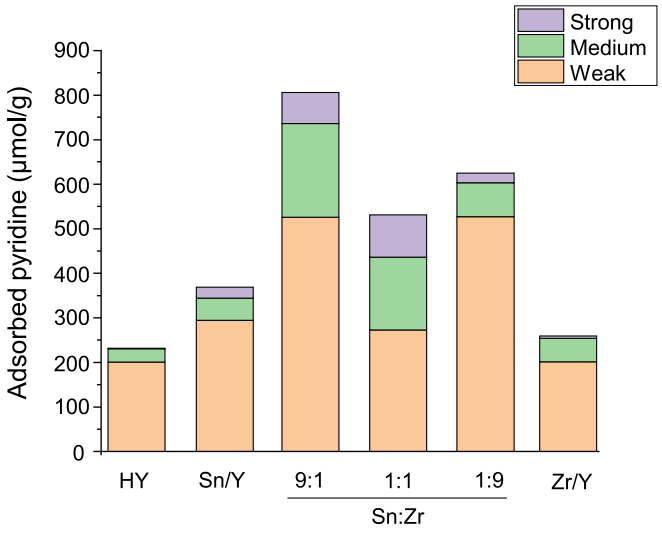

Fig. 4. Total acidity obtained by pyridine adsorption and types of centers (weak, medium and strong) from the catalysts and support before and after of being treated.

or in Zr (SnZr/Y(1:9)) apart from dispersed species, "bulk" metal oxide nanoparticles of SnO_2 and ZrO_2 can be clearly appreciated (Figure S5).

In order to determine the acidity of the catalysts and quantify the Lewis acid sites (LAS) and Brønsted acid sites (BAS), FTIR analysis of adsorbed pyridine was carried out.

Firstly, the total acidity of the samples was determined by the total adsorbed pyridine (Table 2). When the metal is added to the support an increase of the total acidity was detected, which is more pronounced with Sn (368.6 $\mu mol_{pir}/g$) than with Zr (259.0 $\mu mol_{pir}/g$). Moreover, in the case of bimetallic catalysts, the total acidity was much higher than that in monometallic catalysts. The total acidity of catalysts with Sn:Zr ratio of 9:1 and 1:9 was very significant (805.2 and 624.9 $\mu mol_{pir}/g$), respectively. In the case of the bimetallic catalyst with a Sn:Zr molar ratio of 1:1, the amount of adsorbed pyridine was lower (530.6 $\mu mol_{pir}/g$).

In addition, the type of acid sites (weak, medium or strong) can be assigned according to the desorption temperature. Pyridine is released from weak acid sites when the temperature rises to 100 °C. When the temperature is increased up to 200 °C, the pyridine is desorbed from the sites with intermediate acidity whereas those that remain bound to the pyridine at temperatures higher than 200 °C can be considered as strong acid sites. According to the obtained results, most of the catalysts present a majority of weak acid sites with respect to medium and strong sites (Fig. 4). However, bimetallic catalysts, especially SnZr/Y(1:1) and SnZr/Y(9:1), exhibit a larger amount of medium and strong acid sites. Maybe, the weak acidity can be due to the species outside the structure.

Finally, the relationship between Brønsted and Lewis acid sites (BAS/LAS) was estimated by the FTIR spectra of pyridine adsorption. Fig. 5 shows the bands near 1600 and 1445 cm^{-1} which are related to the adsorption of pyridine on LAS, while the band near 1545 cm^{-1} is related to the presence of BAS on the catalyst [65]. There is also a band around 1490 cm^{-1} that corresponds to the presence of both LAS and BAS [47]. In the spectra of adsorbed pyridine, it can be observed that as the temperature increases, the bands corresponding to the pyridine adsorbed in the acid sites decrease due to the desorption process, until reaching a temperature of 200 °C at which almost all the pyridine is eliminated from these sites. With these data, it is possible to establish the amount of BAS and LAS (and therefore their ratio) for the different samples

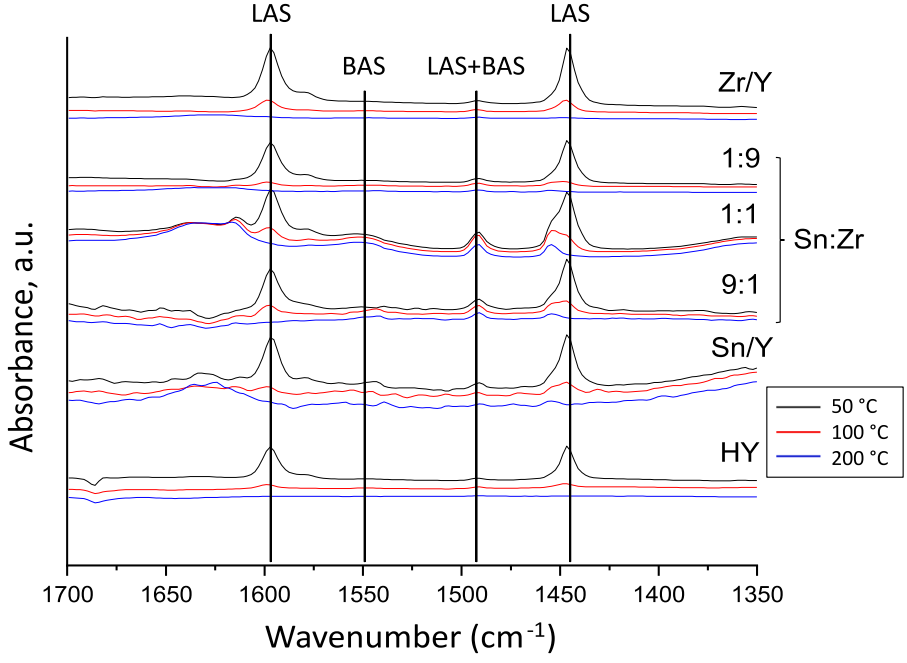

Fig. 5. FTIR spectra of adsorbed pyridine at different temperatures of the catalysts and support before and after of being treated. LAS = Lewis acid sites and BAS = Brønsted acid sites.

Table 3
Chemical compositions obtained by XPS analysis.[a]

Catalyst	C	O	Si	Sn	Zr
Sn/Y	4.37	62.16	32.36	1.11	N.D.
SnZr/Y(9:1)	6.06	61.76	30.73	1.45	< 0.10
SnZr/Y(1:1)	8.10	59.75	26.91	3.26	1.98
SnZr/Y(1:9)	14.75	56.64	25.16	0.35	3.10
Zr/Y	6.93	62.25	26.74	N.D.	3.93

[a] At. % obtained from quantitative analysis (standard deviations less than 0.02 %) of XPS surveys acquired at equivalent experimental conditions (see experimental section for details) from the following core levels: C*1s*, O*1s*, Si*2p*, Sn*3d*, Zr*3p*. N.D.: Not Detected.

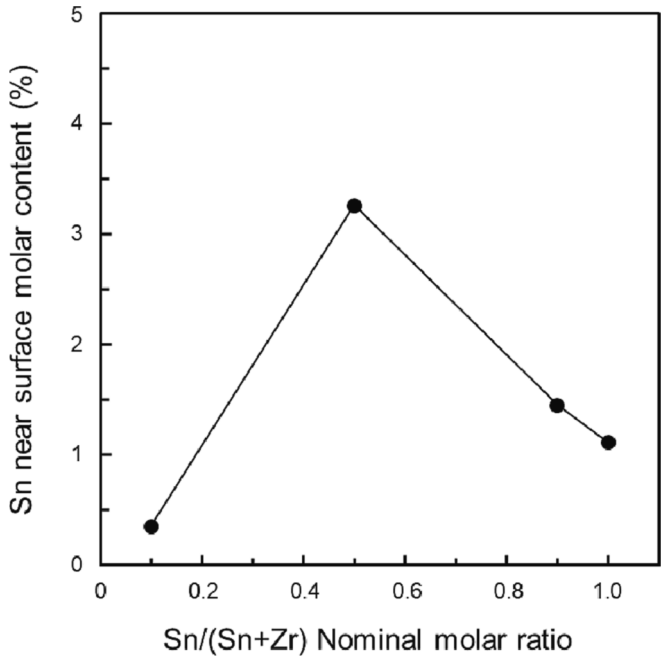

Fig. 6. Variation of Sn near surface content (at.%) on the final catalysts, determined by XPS, with the Sn/(Sn + Zr) at. ratio employed for doping the HY zeolite.

(Table 2). The dealuminated zeolite support has a low BAS/LAS ratio (0.02) that increases upon the incorporation of metals. The addition of only Sn to the support leads to a higher BAS/LAS ratio than when just Zr was added. The catalyst that presented the highest BAS/LAS ratio (0.187) was the bimetallic catalyst with the same content of Sn and Zr (SnZr/Y(1:1)) followed by the bimetallic ones with higher Sn-loading (0.118 for SnZr/Y(9:1)). In contrast, the monometallic Zr catalyst (Zr/Y) presented a relatively low BAS/LAS ratio (0.007). The highest proportion of Brønsted acid sites can be related to the higher dispersion of the Sn and Al species, which are better introduced into the dealumination vacancies, thus generating more Brønsted sites.

These samples were also characterized by XPS and the results from the quantitative analysis of chemical composition near surface of the studied catalysts are shown in Table 3. Oxygen is the most abundant element near surface in all cases, followed by silicon. The amount of carbon is quite low, most likely due to the annealing treatment in air at 500 °C. Finally, the lowest content near surface corresponds to Sn and/or Zr. With respect to Zr, the highest content near surface (ca. 3.9%) appears as expected for the catalyst impregnated with the highest amount of Zr, i.e., without Sn. As expected, this content decreases increasing the Sn/(Sn + Zr) nominal molar ratio employed for impregnation, until the sample doped with Sn/(Sn + Zr) at. ratio of 0.9 for which Zr was hardly detected by XPS. However, this general trend is different for Sn, whose maximum content near surface (ca. 3.3%) appears in the catalyst doped with Sn/(Sn + Zr) nominal molar ratio of 0.5 (Fig. 6). This data is remarkable considering that the bulk chemical analysis indicates that there is the same amount of Zr and Sn atoms, confirming a high dispersion of both Zr and, especially, Sn on the surface of the zeolite support. The amount drops to less than half for Sn/(Sn + Zr) ratios above or below 0.5, and even for the catalyst doped just with Sn.

From a curve fitting analysis performed over the Sn$3d_{5/2}$ region, two main components are found at 485.5 and 487.8 eV for all the catalysts doped with Sn (Fig. 7, left). The minor component at 485.5 eV can be assigned to Sn^{2+} species [66], but this maximum is shifted 2.3 eV below the lower limit reported for the binding energy of regular Sn-O phases. Thus, the component at 485.5 eV fits with the binding energy described for Sn^{2+} species bonded to carbon [66,67]. With respect to the major component, the maximum at 487.8 eV appears ca. 0.6 eV above the limit binding energy reported for pure SnO_2 [68,69]. Indeed, the higher binding energy has been described for Sn^{4+} cations in tetrahedrally coordinated sites from zeolite frameworks [70–72]. This seems to be in good agreement with the low content of Sn species found near surface for most of the catalysts doped with Sn, and both facts suggest a partial incorporation or dilution of Sn species into the HY-zeolite framework. However, the binding energy remains invariable at 487.8 eV in the catalyst doped with Sn/(Sn + Zr) nominal molar ratio of 0.5 (SnZr/Y (1:1), i.e., the one presenting the highest Sn content near surface (Fig. 6 and Table 3). At first sight, this latter fact could be seen as inconsistent. Nevertheless, the 487.8 eV binding energy has been also reported for Sn^{4+} species involved in Sn-O-Zr bonds [70,71], which would explain the inverted situation regarding the high amount of Sn near surface detected for this catalyst (Sn/Zr = 1). Accordingly, the maximum for the Zr$3d_{5/2}$ line in the catalysts containing both, Sn and Zr, appears shifted to higher binding energy, at 183.1 eV, compared to the upper limit of 282.5 eV registered for pure ZrO_2 [68,70,71,73]. Indeed, the 183.1 eV binding energy is within the 182.8–184.2 eV range reported for Zr^{4+} species involved in Zr-O-Sn bonds [70,71]. By contrast, the maximum for the Zr$3d_{5/2}$ line in the catalyst doped just with Zr is centered at 182.3 eV, which is consistent with the binding energy reported for pure ZrO_2 [68,70,71,73].

3.2. Catalytic results

The catalytic conversion of FF into GVL was carried out in one-pot with the different Zr- or Sn-supported catalysts using 2-propanol as a hydrogen donor (MPV reduction). The main reaction products observed were γ-valerolactone (GVL), furfuryl ether (FE), furfuryl alcohol (FAL) and isopropyl levulinate (IPL). Other reaction products such as polymers of furfural and furfuryl alcohol have been also detected (intermediate products such as α-angelica lactone and other products such as 3-penten-1-ol, 2-ciclopenten-1-one, 1,4-pentanediol and 2-pentenoic acid were also detected).

Previously, a blank run without catalyst was carried out at 180 °C for 3 h. In these conditions a FF conversion of 7% was achieved but no GVL was produced. Therefore, all the GVL production must be related to the presence of the catalysts.

For comparison, using the same reaction conditions, further reactions employing the undoped HY support, pure ZrO_2 and pure SnO_2 were also carried out. When the support (HY) is used in the reaction, FF conversion of 71.5 % was detected but no yield to GVL was observed. In this case the main reaction product observed was IPL. This result was similar to that obtained with the zeolite before treatment (Al-HY), where a 81.5 % of furfural conversion was achieved, without GVL production. These catalysts require Brønsted-type acidity to open the furan ring and form alkyl levulinates. On the other hand, when unsupported ZrO_2 or SnO_2 were used in the reaction FF conversion greater than 95 % was reached, but no yield to GVL was observed (Fig. 8). For these catalysts, the main reaction product was FAL, which is obtained on Lewis acid sites.

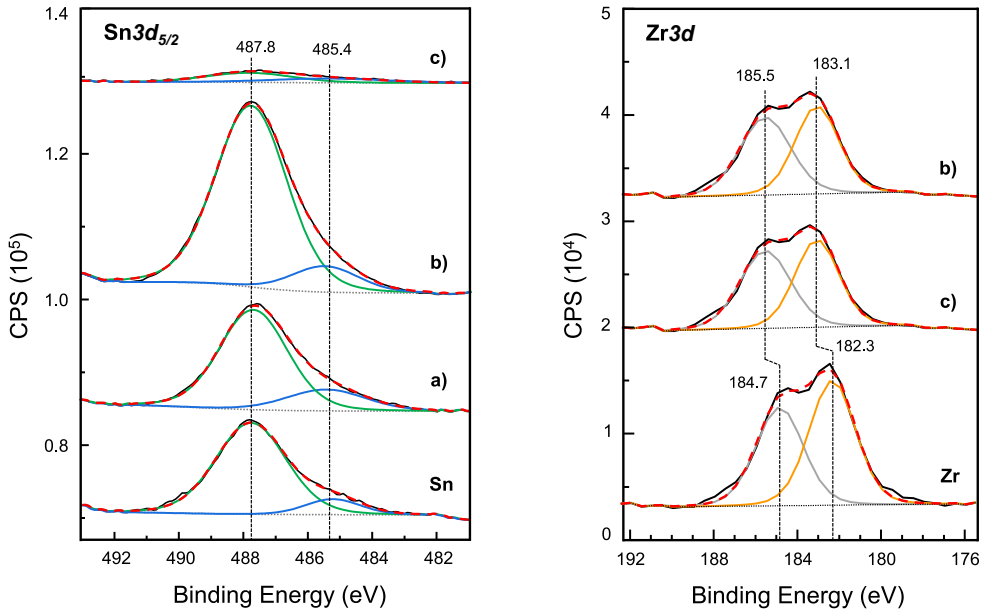

Fig. 7. X-ray photoelectron spectra of Sn$3d_{5/2}$ (left), Zr*3d* (center) and Si*2p* (right) regions from samples doped with Sn, Zr, or different Sn/(Sn + Zr) nominal molar ratio: 0.9 (a), 0.5 (b), and 0.1 (c). Sn corresponds to Sn/Y catalyst. Zr corresponds to Zr/y catalyst. Curve fitting analysis is included for the Sn$3d_{5/2}$ region. Note: negligible intensity was detected in Zr*3d* region for the spectrum from sample doped with Sn/(Sn + Zr) nominal molar ratio of 0.9 (a).

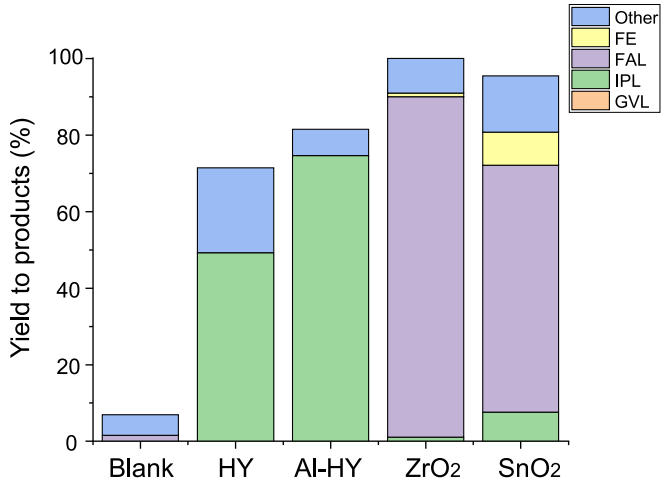

Fig. 8. Yield to products using metallic oxides (ZrO_2 y SnO_2), zeolite Y before (Al-HY-15) and after treatment (HY-15), and blank reaction without catalyst. Reaction conditions: 0.25 mmol of furfural in 5 mL of 2-propanol, 0.2 g of catalyst, at 180 ° for 3 h.

Interestingly, all the supported catalysts obtained high FF conversions exceeding 99%, and, unlike the former samples, elevated yields to GVL (Fig. 9). Thus, after 3 h, the supported monometallic catalysts (Sn/Y and Zr/Y) produced a yield to GVL of 70 and 68 % respectively with significant formation of IPL. For a proper analysis and comparison of the data, reaction at lower conversions for 1 h was used for further experiments. In this case, the yield to GVL was 38 and 34% for Sn/Y and Zr/Y, respectively.

When bimetallic catalysts were used in the reaction, the yield to GVL highly increased compared to monometallic catalysts (Fig. 9). Then, a clear synergetic effect between Sn and Zr was observed. The highest yield to GVL was obtained with the catalyst with the same amount of Sn and Zr (SnZr/Y(1:1)) achieving, after 1 h, a yield to GVL of 78%. This catalyst, despite having less acidity to activate the FF molecule and the reaction intermediates, produces more GVL. The lactonization reaction to obtain GVL requires a relatively high temperature and is favored by the presence of Brønsted-type acidity. Since the SnZr/Y (1:1) catalyst presents a higher proportion of Brønsted acid sites, it can enhance the formation of a greater amount of products at relatively short times. Apart from these catalyst, samples with Sn/Zr atomic ratios of 3:1 and 1:3 were also synthesized and tested in the furfural transformation. Both catalysts showed higher yields to GVL than pure Zr or Sn, but lower than the 1:1 ratio (being 62.2 and 67.6 % of GVL using Sn/Zr atomic ratios of

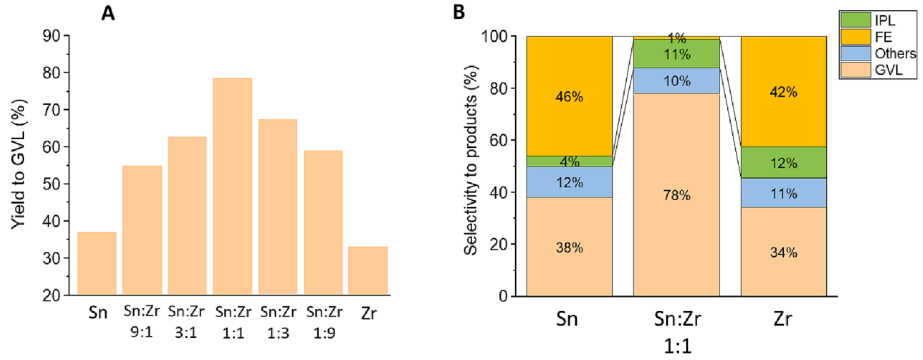

Fig. 9. Yield to GVL (A) and selectivity to products (B) using catalysts based on Sn, Zr and bimetallic with different Sn:Zr molar ratios (9:1; 1:1; 1:9) supported on dealuminated zeolite Y (HY). Reaction conditions: 0.25 mmol of furfural in 5 mL of 2-propanol, 0.2 g of catalyst, at 180 ° for 1 h.

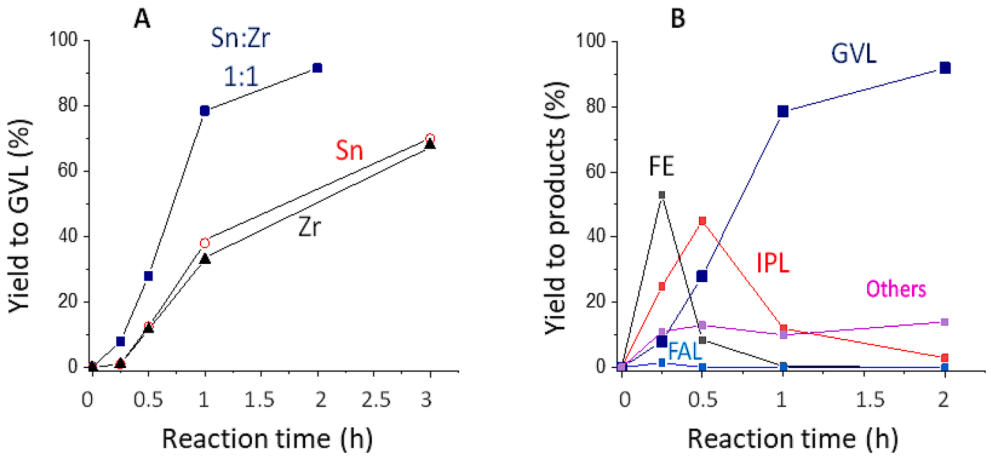

Fig. 10. Evolution of the yield to GVL with the reaction time for Sn/Y (○), Zr/Y (□) and SnZr/Y (1:1) (■) catalysts (Fig. 10A). Variation of the yields to different reaction products with the time on line using SnZr/Y(1:1) catalyst (Fig. 10B). Symbols in Fig. 10B: γ-valerolactone (GVL, ■), isopropyl levulinate (IPL, ■), furfuryl alcohol (FAL, ■), furfuryl ether (FE, ■) and others (■). Reaction conditions: 0.25 mmol of furfural in 5 mL of 2-propanol, 0.2 g of catalyst, at 180 ºC.

3:1 and 1:3, respectively).

Results shown in Fig. 9 compare yields and selectivities at ca. 100% of FF conversion. Then, experiments using low amounts of catalyst and short reaction times were conducted in order to properly compare the reactivity of the active sites of the different catalysts. Table S1 shows the results of the catalytic activity, specific activity per surface area and the catalytic activity per metal-site. Just using the support, the furfural molecule can be easily activated, but as observed in Fig. 8, no GVL was formed. Pure oxides (ZrO_2 and SnO_2) showed low catalytic activity, but a relatively high specific activity due to their low surface area. The monometallic catalysts, Sn/Y and Zr/Y, presented a high catalytic activity, 0.0327 and 0.0256 $mol_{FF}\ h^{-1}\ g_{cat}^{-1}$, respectively. The bimetallic catalyst with the same amount of Sn and Zr atoms (SnZr/Y(1:1)) presented higher catalytic activity than the monometallic ones. If it is taken into account the activity per metal site, the bimetallic catalyst has the highest reactivity. Thus, a clear synergistic effect when both metals are added into the support is confirmed.

The influence of the reaction time on the yield to GVL (Fig. 10A) was studied for monometallic catalysts as well as for the optimal bimetallic catalyst (SnZr/Y(1:1)). Interestingly, the highest differences were observed for low reaction times. Then, after 15 min, the yield to GVL with the bimetallic catalysts was ca. 8% whereas for the monometallic samples the yield did not reach 2%. After just 2 h of reaction, the bimetallic catalyst showed a yield to GVL close to 90%, while the Sn/Y and Zr/Y catalysts produced yields to GVL lower than 65% after 3 h.

Fig. 10B shows the different yields to products achieved at different reaction times using the most efficient catalyst (SnZr/Y(1:1)). For comparison, Figure S6 plots the formation of the different products with reaction time for monometallic supported catalysts. The intermediary products presented higher yields at shorter reaction times when the monometallic catalysts were used. Differently, when the bimetallic catalyst is used the yield to intermediary products decreased until a low level after only 1 h of reaction, producing mainly GVL as a reaction product. Additionally, for the bimetallic catalyst, the cascade reaction to transform FF into GVL takes place faster.

4. Discussion

The catalyst that obtained the best catalytic performance and produced the highest GVL yield was the bimetallic catalyst with the same amount of Zr and Sn atoms. The main physicochemical feature of this catalyst is the elevated dispersion of the ZrOx and, especially, of the SnOx species on the surface of the zeolitic support, as confirmed by XPS, XRD, DR-UV–Vis. and TEM measurements. Thus, a high Sn-concentration has been observed in the optimal sample. The Zr-free catalyst possesses a Sn/Si = 0.034 on the near surface whereas in the optimal bimetallic catalyst, the Sn/Si ratio increases until 0.12, in spite of presenting half of the Sn concentration in its composition in comparison to that of the monometallic catalyst. Moreover, according to the microscopy analysis, both Zr and Sn are closely located. Although a mixed Sn-Zr-O crystalline phase has not been detected by XRD, surface Sn^{4+} species involved in Sn-O-Zr bonds are predominant on the surface of the catalyst (XPS).

In spite of presenting an excellent dispersion, the optimal catalyst also has the highest proportion of Brønsted acid sites (higher BAS/LAS ratio). Therefore, apart from a great interaction metal/support, a higher proportion of BAS, a not very strong acidity (as very strong acidity can cause polymerization and formation of humins) and a large proportion

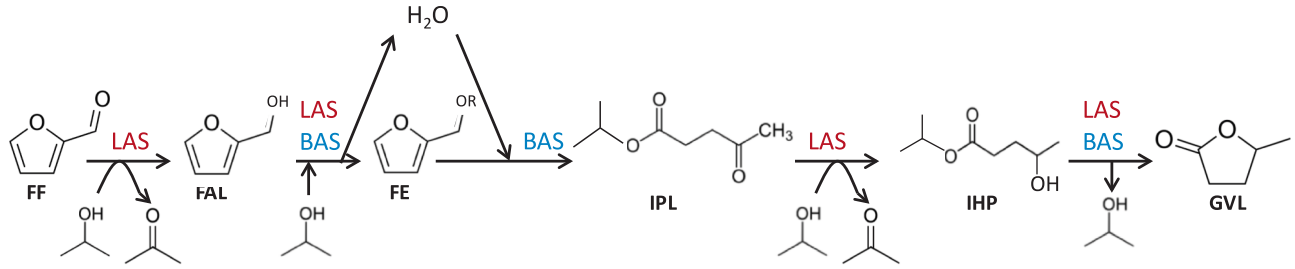

Fig. 11. Proposed reaction mechanism according to the catalytic results obtained.

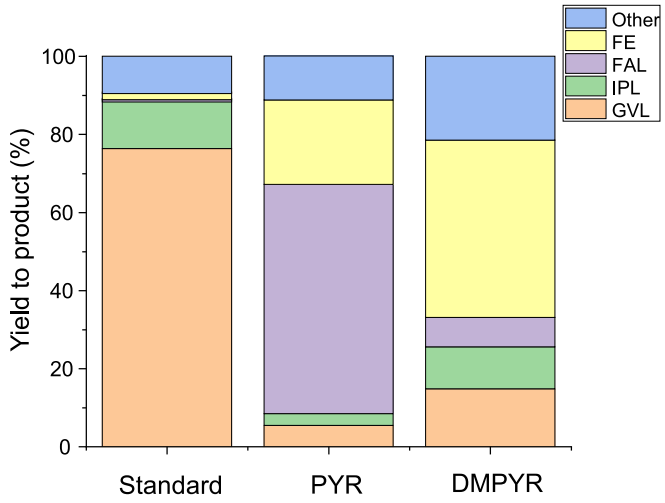

Fig. 12. Furfural conversion over over SnZr/Y(1:1), adding pyridine (PYR) and 2,6-dimetil-pyridine (DMPYR) in order to block LAS and BAS, respectively. Reaction conditions: 0.25 mmol of furfural in 5 mL of 2-propanol, 0.2 g of catalyst, at 180 °C for 1 h. [b]γ-valerolactone (GVL); isopropyl levulinate (IPL); furfuryl alcohol (FAL); furfuryl ether (FE).

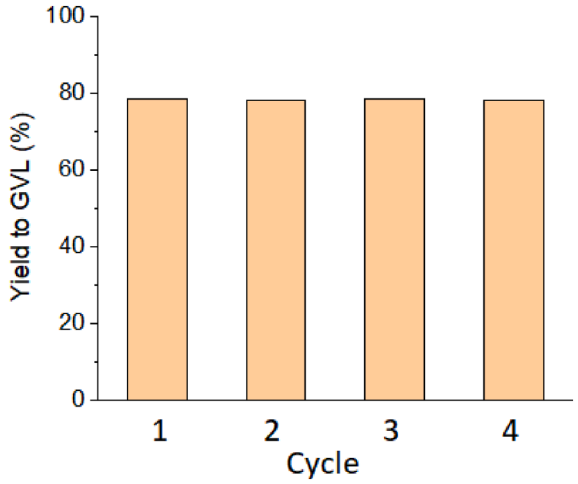

Fig. 13. Yield to GVL from FF upon reusability tests over SnZr/Y(1:1). [a] Reaction conditions: 0.25 mmol of furfural in 5 mL of 2-propanol, 0.2 g of catalyst, at 180 °C for 1 h.

of weak and medium acid sites seem to favor, in this case, the production of GVL from FF. As shown in previous studies [29,52] Brønsted acid centers (BAS) are necessary to carry out alcoholysis and cyclization reactions, but an excess of BAS promotes the formation of humins. Therefore, an adequate BAS/LAS ratio, but predominating LAS, favor the efficient conversion of FF to GVL.

It is known that the existence of both Brønsted and Lewis acid sites is necessary for an optimized catalytic performance in the overall FF to GVL reaction. However, the ratio between both types of acid sites has to be controlled and not all the acid sites are equally efficient. For example, pure zeolites before the dealuminization process, present both Brønsted and Lewis acid sites but, in our conditions, hardly yield valerolactone. Therefore, the presence of metals like those of Zr or Sn, that induces the formation of Lewis acid sites, are strictly required.

In Fig. 11, a reaction mechanism could be proposed according to the results obtained [43,74]. Firstly, FF is transformed into FAL, promoted by LAS. Then, FAL can react with the alcohol to form FE, which can be transformed into IPL by hydrolysis, BAS being essential for the transformation of FE into IPL. IPL is transformed into alkyl 4-hydroxy-pentanoate by another hydrogenation step and later to GVL by cyclation. Therefore, LAS and BAS are necessary to carry out the reactions to form GVL from FF. Finally, the lactonization step is the one that requires harder reaction conditions, i.e. higher temperatures or longer times.

In order to establish a relationship between the different types of acid sites, experiments with pyridine (PYR) and 2,6-dimetyl-pyridine (DMPYR) added to the reaction media (with a molar ratio with FF of 1:1) were carried out using the optimal SnZr/Y(1:1) catalyst. The purpose of these experiments is to understand the role of BAS and LAS on the reaction mechanism. Thus, PYR adsorbs (blocking) on both Lewis (LAS) and Brønsted acid sites (BAS) whereas DMPYR adsorbs (blocking) Brønsted acid sites (BAS), [75,76]. Fig. 12 shows that the yield to GVL was very low when these compounds were added to the reaction media. Then, using pyridine the yield to GVL did not exceed 5% with a large selectivity to furfuryl alcohol (FAL). When pyridine is adsorbed, the catalysts are less active because the Lewis and Brønsted sites are blocked, thus leaving the one-pot reaction in earlier stages. In principle, if pyridine adsorption was complete, all sites should be blocked but, however, reactivity is observed. This might be explained due to the fact that basic sites are involved in the reaction [74,77] or, more likely, because at 180 °C a part of the adsorbed pyridine is desorbed and some sites remain available.

When 2,6-dimetyl-pyridine was used, the yield to GVL was of ca. 15%, mainly leading to the formation of furfuryl ether (FE). On the one hand, the experiment with pyridine, which tries to block both types of acid sites (necessary for the first step: FF to FAL), finished in the FAL formation. On the other hand, the addition of 2,6-dimetyl-pyridine, that tends to block Brønsted acid sites, implies a higher degree of FF transformation to GVL (Fig. 12), due to the fact that the first step (FF to FAL) is not apparently hindered. When, 2,6-dimetyl-pyridine is used, a higher amount of FE, IPL and GVL is observed. As the Lewis sites become available, the reaction proceeds further. As indicated above for pyridine, it is likely that part of the DMPYR that blocks the Brønsted sites is desorbed at that temperature, which is the reason why IPL and subsequent one-pot reaction products are observed. These results show that both types of sites are essential to produce GVL from FF, otherwise very low yields to GVL are achieved.

To evaluate the influence of the reaction temperature on the catalytic performance (Figure S7), three different temperatures (120, 150 and 180 °C) were tested using the same reaction conditions (reaction time of 1 h). Thus, a strong effect on the yield to products is observed. Although for all the experiments the furfural conversion is ca. 100%, if the reaction is carried out at lower temperatures, longer reaction times to obtain high yields to GVL are required. That is; at 120 °C a GVL yield of 13.2% was achieved, while higher yields to FE and IPL were also detected. When the reaction takes place at 150 °C the yield to GVL increases until 42.3% and the yield to FE is reduced to 1.4%, producing also a 37% of yield to IPL. Apparently, higher temperatures favor ring opening, the transformation of FE into IPL and the cyclation and hydration process from IPL to GVL. As it can be observed at 150 °C after 1 h of reaction, the yield to IPL is very high, but, for longer reaction times (3 h), this yield decreases. Therefore, as expected, longer reaction times are necessary for the transformation of IPL into GVL at lower temperatures. It must be pointed out that the pattern of the reaction products obtained at 120, 150 or 180 °C is not exactly the same. Then, a GVL yield of ca. 45% is achieved after 3 h at 120 °C, after 1 h at 150 °C and after 0.6 h at 180 °C. In all cases, although IPL is the most abundant co-product, an increase in the reaction temperature promotes the formation of GVL and the decrease of other byproducts.

To evaluate the catalyst reusability, a recycling test on the production of GVL from FF was carried out with the SnZr/Y(1:1) catalyst. Commonly, the reused catalyst was separated from the products by filtration. Then the catalyst was washed with distillated water and dried in an oven at 120 °C overnight before reuse. It was observed that, after 4 cycles, the catalyst maintained its catalytic activity, showing the same yield to GVL (Fig. 13). This indicates that the catalysts can be reused

Table 4
Representative results in the furfural transformation into γ-valerolactone.

Furfural [M]	Catalyst	Solvent	Hydrogen source	T (°C)	Time (h)	Yield to GVL (%)	Reference
0.04	Au/ZrO_2 + ZSM-5	2-propanol	2-propanol	120	30	80.4	[46]
0.45	Zr-Beta + Al-MFI	2-butanol/water	2-butanol	120	48	78	[53]
0.05	Meso Zr-Al-Beta	2-propanol	2-propanol	120	24	95	[62]
0.2	Zr-HY + Al-HY	2-pentanol	2-pentanol	120	5	85	[47]
0.4	Zr-HY + Al-HY	2-pentanol	2-pentanol	120	10	78	
0.26	ZrO_2-SBA-15	2-propanol	2-propanol	170	7	37	[55]
0.11	Sn-Al Beta	2-propanol	2-propanol	180	24	60	[50]
0.17	CuAl + H-ZSM-5	ethanol	Molecular hydrogen	160	4	90.5	[77]
0.2	Zr/Silica	2-propanol	2-propanol	200	6	40.8	[78]
0.05	Fe_3O_4/ZrO_2@MCM-41	2-propanol	2-propanol	150	30	85	[79]
0.2	FM-Zr-ARS	2-propanol	2-propanol	160	8	72.4	[40]
0.4	Chitosan-Ru/ZSM-5 + PPh3	ethanol	Formic acid	160	30	79	[80]
0.3	$AuRu/Y–ZrO_2$	2-propanol	2-propanol	150	5	71	[41]
0.1	VPA-Hf	2-propanol	2-propanol	180	14	81	[81]
0.05	ZrSn/Y(1:1)	2-propanol	2-propanol	180	1	78	This work

without losing catalytic activity. The chemical analysis after 4 cycles shows that the content of Sn and Zr hardly changed compared to the fresh catalyst, which can be the reason for its high stability. This absence of metal leaching must be due to the strong cleavage of the highly dispersed Sn-Zr-O species on the surface of the catalyst.

The results obtained in the present article have been compared with others reported in the literature. The yields to GVL obtained in this work are amongst the highest, especially highlighting the short reaction time used (Table 4).

Finally, the optimal catalyst, SnZr/Y(1:1), was selected to test its ability to produce GVL from other biomass-derived compounds such as levulinic acid (LA), methyl levulinate (ML) and ethyl levulinate (EL) (Table S2). It was detected that LA and EL achieved almost full conversion and excellent yield to GVL (86.4 % and 84.6 %, respectively), which confirms the excellent ability of the bimetallic SrZn catalyst to obtain γ-valerolactone from different biomass derived substrates.

5. Conclusions

A clear synergistic effect between Sn and Zr has been observed in the furfural transformation into γ-valerolactone. Thus, bimetallic Sn-Zr catalysts supported on zeolite Y with a dealumination treatment reaches remarkably higher γ-valerolactone formation than monometalic Sn or Zr catalyst, especially when the Sn:Zr at. ratio is 1. We must remark that at low reaction times the γ-valerolactone formation employing the optimal bimetallic catalyst is 4-fold that of the monometallic catalysts. The improvement in the catalytic activity could be due to the high dispersion of Sn and Zr species on the support through the formation of dispersed mixed surface Sn-O-Zr species, this way allowing a high number of available active sites. Because of the need for Lewis and Brønsted acid sites for the multistep furfural transformation into γ-valerolactone, the fact that the optimal catalyst has the highest Brønsted to Lewis sites ratio can be linked to the higher γ-valerolactone formation. Interestingly, the optimal bimetallic catalyst showed a high stability since after 4 reaction cycles the catalyst gave the same yield to γ-valerolactone than in the first cycle and the chemical analysis revealed that the metal leaching was negligible. This high stability must be due to the good interaction between the metals species and the support due to an elevated dispersion of the metallic species.

CRediT authorship contribution statement

Adrián García: Investigation, Writing – original draft. **Rita Sánchez-Tovar:** Funding acquisition, Resources, Validation. **Pablo J. Miguel:** Investigation, Methodology. **Elena Montejano-Nares:** Investigation, Visualization. **Francisco Ivars-Barceló:** Investigation, Resources. **Juan Antonio Cecilia:** Investigation, Resources. **Benjamín Torres-Olea:** Funding acquisition, Supervision, Writing – review & editing. **Benjamín Solsona:** Funding acquisition, Supervision, Writing – review & editing.

Declaration of Competing Interest

The authors declare that they have no known competing financial interests or personal relationships that could have appeared to influence the work reported in this paper.

Data availability

Data will be made available on request.

Acknowledgements

Authors gratefully acknowledge the financial support by the Ministerio de Ciencia e Innovación of Spain (MINECO/FEDER) through the projects TED2021-129555B-I00 and PID2021-1262350B-C33, FEDER Una manera de hacer Europa and the pre-doctoral grant PRE2018-085211 (AG). Authors also thank the Generalitat Valenciana for CIAICO/2021/094 and CIGRIS/2022/198. FIV acknowledges the support from "Ramón y Cajal" excellence program (Ref.: RYC2020-029470-I/AEI/10.13039/501100011033). EMN acknowledges the support from the predoctoral fellowship UNED-Santander.

Appendix A. Supplementary data

Supplementary data to this article can be found online at https://doi.org/10.1016/j.fuel.2023.129045.

References

[1] Perea-Moreno MA, Samerón-Manzano E, Perea-Moreno AJ. Biomass as renewable energy: Worldwide research trends. Sustainability 2019;11(3):863.
[2] Raj T, Chandrasekhar K, Banu R, Yoon J-J, Kumar G, Kim S-H. Synthesis of γ-valerolactone (GVL) and their applications for lignocellulosic deconstruction for sustainable green biorefineries. Fuel 2021;303.
[3] Oubraham A, Zaccour G. A survey of applications of viability theory to the sustainable exploitation of renewable resources. Ecol Econ 2018;145:346–67.
[4] Zhang H, Chen L, Li Y, Hu Y, Li H, Xu CC, et al. Functionalized organic-inorganic hybrid porous coordination polymers based catalysts for biodiesel production via trans/esterification. Green Chem 2022;24:7763–86.
[5] Zhang H, Li Hu, Xu CC, Yang S. Heterogeneously chemo/enzyme-functionalized porous polymeric catalysts of high-performance for efficient biodiesel production. ACS Catal 2019;9(12):10990–1029.
[6] Lee CBTL, Wu TY, Yong KJ, Cheng CK, Siow LF, Jahim JM. Investigation into Lewis and Brønsted acid interactions between metal chloride and aqueous choline chloride-oxalic acid for enhanced furfural production from lignocellulosic biomass. Sci Total Environ 2022;827.
[7] Ho MC, Ong VZ, Wu TY. Potential use of alkaline hydrogen peroxide in lignocellulosic biomass pretreatment and valorization–a review. Renew Sust Energ Rev 2019;112:75–86.

[8] Wyman CE, Dale BE, Elander RT, Holtzapple M, Ladisch MR, Lee YY. Coordinated development of leading biomass pretreatment technologies. Bioresour Technol 2005;96(18):1959–66.
[9] Hernández B, Iglesias J, Morales G, Paniagua M, López-Aguado C, Fierro JLG, et al. One-pot cascade transformation of xylose into γ-valerolactone (GVL) over bifunctional Brønsted-Lewis Zr–Al-beta zeolite. Green Chem 2016;18(21):5777–81.
[10] Ye L, Han Y, Feng J, Lu X. A review about GVL production from lignocellulose: Focusing on the full components utilization. Ind Crop Prod 2020;144.
[11] Mahmood H, Moniruzzaman M, Iqbal T, Khan MJ. Recent advances in the pretreatment of lignocellulosic biomass for biofuels and value-added products. Curr Opin Green Sustain Chem 2019;20:18–24.
[12] La C-S. biomasa–fuente alternativa de combustibles y compuestos químicos. Anales de Química de la RSEQ 2019;115(5):399.
[13] Nikolla E, Román-Leshkov Y, Moliner M, Davis ME. "One-pot" synthesis of 5-(hydroxymethyl) furfural from carbohydrates using tin-beta zeolite. ACS Catal 2011;1(4):408–10.
[14] Sakakibara K, Endo K, Osawa T. Facile synthesis of γ-valerolactone by transfer hydrogenation of methyl levulinate and levulinic acid over Ni/ZrO2. Catal Commun 2019;125:52–5.
[15] Luo Y, Li Z, Li X, Liu X, Fan J, Clark JH, et al. The production of furfural directly from hemicellulose in lignocellulosic biomass: A review. Catal Today 2019;319:14–24.
[16] Khan AS, Man Z, Bustam MA, Kait CF, Nasrullah A, Ullah Z, et al. Dicationic ionic liquids as sustainable approach for direct conversion of cellulose to levulinic acid. J Clean Prod 2018;170:591–600.
[17] García A, Sanchis R, Miguel PJ, Dejoz AM, Pico MP, López ML, et al. Low temperature conversion of levulinic acid into γ-valerolactone using Zn to generate hydrogen from water and nickel catalysts supported on sepiolite. RSC Adv 2020;10(35):20395–404.
[18] Gürbüz EI, Gallo JMR, Alonso DM, Wettstein SG, Lim WY, Dumesic JA. Conversion of hemicellulose into furfural using solid acid catalysts in γ-valerolactone. Angew Chem 2013;52(4):1270–4.
[19] Tang X, Zeng X, Li Z, Hu L, Sun Y, Liu S, et al. Production of γ-valerolactone from lignocellulosic biomass for sustainable fuels and chemicals supply. Renew Sust Energ Rev 2014;40:608–20.
[20] Yan K, Yang Y, Chai J, Lu Y. Catalytic reactions of gamma-valerolactone: A platform to fuels and value-added chemicals. Appl Catal B 2015;179:292–304.
[21] Wang H, Wu Y, Li Y, Peng J, Gu X-K, Ding M. One-step synthesis of gasoline fuels from γ-valerolactone with high selectivity over Cu/HZSM-5 bifunctional catalyst. Appl Catal B 2021;296.
[22] García A, Sanchis R, Llopis FJ, Vázquez I, Pico MP, López ML, et al. Ni supported on natural clays as a catalyst for the transformation of levulinic acid into γ-valerolactone without the addition of molecular hydrogen. Energies 2020;13(13):3448.
[23] Belguendouz MNEH, Gancedo J, Rapado P, Ursueguía D, Patiño Y, Faba L, et al. Selective synthesis of γ-valerolactone from levulinic and formic acid over ZnAl mixed oxide. Chem Eng J 2021;414.
[24] De Graauw CF, Peters JA, Van Bekkum H, Huskens J. Meerwein-Ponndorf-Verley reductions and Oppenauer oxidations: an integrated approach. Synthesis 1994;1994(10):1007–17.
[25] García A, Miguel PJ, Pico MP, Álvarez-Serrano I, López ML, García T, et al. γ-valerolactone from levulinic acid and its esters: Substrate and reaction media determine the optimal catalyst. Appl Catal A 2021;623.
[26] Cai B, Zhou XC, Miao YC, Luo JY, Pan H, Huang YB. Enhanced catalytic transfer hydrogenation of ethyl levulinate to γ-valerolactone over a robust Cu–Ni bimetallic catalyst. ACS Sustain Chem Eng 2017;5(2):1322–31.
[27] Shao Y, Ba S, Sun K, Gao G, Fan M, Wang J, et al. Selective production of γ-valerolactone or 1, 4-pentanediol from levulinic acid/esters over Co-based catalyst: Importance of the synergy of hydrogenation sites and acidic sites. Chem Eng J 2022;429.
[28] Douthwaite M, Zhang B, Iqbal S, Miedziak PJ, Bartley JK, Willock DJ, et al. Transfer hydrogenation of methyl levulinate with methanol to gamma valerolactone over Cu-ZrO2: A sustainable approach to liquid fuels. Catal Commun 2022;164.
[29] Li W, Li M, Liu H, Jia W, Yu X, Wang S, et al. Domino transformation of furfural to γ-valerolactone over SAPO-34 zeolite supported zirconium phosphate catalysts with tunable Lewis and Brønsted acid sites. Mol Catal 2021;506.
[30] He O, Zhang Y, Wang P, Liu L, Wang Q, Yang N, et al. Experimental and kinetic study on the production of furfural and HMF from glucose. Catalysts 2021;11(1):11.
[31] Fang X, Andersson MP, Wang Ze, Song W, Li S. Density functional theory study on the initial reactions of D-xylose and D-xylulose dehydration to furfural. Carbohydr Res 2022;511.
[32] Du XL, He L, Zhao S, Liu YM, Cao Y, He HY, et al. Hydrogen-Independent reductive transformation of carbohydrate biomass into γ-valerolactone and pyrrolidone derivatives with supported gold catalysts. Angew Chem 2011;50(34):7815–9.
[33] Ershova O, Nieminen K, Sixta H. The role of various chlorides on xylose conversion to furfural: Experiments and kinetic modeling. ChemCatChem 2017;9(15):3031–40.
[34] Mariscal R, Maireles-Torres P, Ojeda M, Sádaba I, Granados ML. Furfural: a renewable and versatile platform molecule for the synthesis of chemicals and fuels. Energ Environ Sci 2016;9(4):1144–89.
[35] Wang S, Lin H, Chen J, Zhao Y, Ru B, Qiu K, et al. Conversion of carbohydrates into 5-hydroxymethylfurfural in an advanced single-phase reaction system consisting of water and 1, 2-dimethoxyethane. RSC Adv 2015;5(102):84014–21.
[36] Wang Y, Ding G, Yang X, Zheng H, Zhu Y, Li Y. Selectively convert fructose to furfural or hydroxymethylfurfural on Beta zeolite: The manipulation of solvent effects. Appl Catal B 2018;235:150–7.
[37] Xu Z, Li W, Du Z, Wu H, Jameel H, Chang HM, et al. Conversion of corn stalk into furfural using a novel heterogeneous strong acid catalyst in γ-valerolactone. Bioresour Technol 2015;198:764–71.
[38] Li X, Liu Q, Si C, Lu L, Luo C, Gu X, et al. Green and efficient production of furfural from corn cob over H-ZSM-5 using γ-valerolactone as solvent. Ind Crops and Prod 2018;120:343–50.
[39] Zhu Y, Li W, Lu Y, Zhang T, Jameel H, Chang HM, et al. Production of furfural from xylose and corn stover catalyzed by a novel porous carbon solid acid in γ-valerolactone. RSC Adv 2017;7(48):29916–24.
[40] Peng Q, Wang H, Xia Y, Liu X. One-pot conversion of furfural to gamma-valerolactone in the presence of multifunctional zirconium alizarin red S hybrid. Appl Catal A 2021;621.
[41] Morandi S, Manzoli M, Chan-Thaw CE, Bonelli B, Stucchi M, Prati L, et al. Unraveling the effect of ZrO2 modifiers on the nature of active sites on AuRu/ZrO2 catalysts for furfural hydrogenation. Sustain Energy Fuels 2020;4(3):1469–80.
[42] Li X, Yuan X, Xia G, Liang J, Liu C, Wang Z, et al. Catalytic production of γ-valerolactone from xylose over delaminated Zr-Al-SCM-1 zeolite via a cascade process. J Catal 2020;392:175–85.
[43] García A, Miguel PJ, Ventimiglia A, Dimitratos N, Solsona B. Optimization of the Zr-loading on siliceous support catalysts leads to a suitable Lewis/Brønsted acid sites ratio to produce high yields to γ-valerolactone from furfural in one-pot. Fuel 2022;324.
[44] Sun W, Li H, Wang X, Liu A. Cascade upgrading of biomass-derived furfural to γ-valerolactone over Zr/Hf-based catalysts. Front Chem 2022;10.
[45] Antunes MM, Lima S, Neves P, Magalhães AL, Fazio E, Fernandes A, et al. One-pot conversion of furfural to useful bio-products in the presence of a Sn, Al-containing zeolite beta catalyst prepared via post-synthesis routes. J Catal 2015;329:522–37.
[46] Zhu S, Xue Y, Guo J, Cen Y, Wang J, Fan W. Integrated conversion of hemicellulose and furfural into γ-valerolactone over Au/ZrO2 catalyst combined with ZSM-5. ACS Catal 2016;6(3):2035–42.
[47] Zhang H, Yang W, Roslan II, Jaenicke S, Chuah GK. A combo Zr-HY and Al-HY zeolite catalysts for the one-pot cascade transformation of biomass-derived furfural to γ-valerolactone. J Catal 2019;375:56–67.
[48] Dijkmans J, Dusselier M, Gabriëls D, Houthoofd K, Magusin PC, Huang S, et al. Cøøooperative catalysis for multistep biomass conversion with Sn/Al Beta zeolite. ACS Catal 2015;5(2):928–40.
[49] Melero JA, Morales G, Iglesias J, Paniagua M, Lopez-Aguado C. Rational optimization of reaction conditions for the one-pot transformation of furfural to γ-valerolactone over Zr–Al-beta zeolite: toward the efficient utilization of biomass. Ind Eng Chem Res 2018;57(34):11592–9.
[50] Winoto HP, Ahn BS, Jae J. Production of γ-valerolactone from furfural by a single-step process using Sn-Al-Beta zeolites: Optimizing the catalyst acid properties and process conditions. J Ind Eng Chem 2016;40:62–71.
[51] Maderuelo-Solera R, Richter S, Jiménez-Gómez CP, García-Sancho C, García-Mateos FJ, Rosas JM, et al. Porous SiO2 nanospheres modified with ZrO2 and their use in one-pot catalytic processes to obtain value-added chemicals from furfural. Ind Eng Chem Res 2021;60(51):18791–805.
[52] Kim KD, Kim J, Teoh WY, Kim JC, Huang J, Ryoo R. Cascade reaction engineering on zirconia-supported mesoporous MFI zeolites with tunable Lewis-Brønsted acid sites: A case of the one-pot conversion of furfural to γ-valerolactone. RSC Adv 2020;10(58):35318–28.
[53] Bui L, Luo H, Gunther WR, Román-Leshkov Y. Domino reaction catalyzed by zeolites with Brønsted and Lewis acid sites for the production of γ-valerolactone from furfural. Angew Chem 2013;125(31):8180–3.
[54] Saito M, Aihara T, Miura H, Shishido T. Brønsted acid property of alumina-based mixed-oxides-supported tungsten oxide. Catal Today 2021;375:64–9.
[55] Iglesias J, Melero JA, Morales G, Paniagua M, Hernández B, Osatiashtiani A, et al. ZrO2-SBA-15 catalysts for the one-pot cascade synthesis of GVL from furfural. Cat Sci Technol 2018;8(17):4485–93.
[56] Corma A, Domine ME, Nemeth L, Valencia S. Al-free Sn-beta zeolite as a catalyst for the selective reduction of carbonyl compounds (Meerwein– Ponndorf– Verley reaction). J Am Chem Soc 2002;124(13):3194–5.
[57] Li S, Zheng A, Su Y, Zhang H, Chen L, Yang J, et al. Brønsted/Lewis acid synergy in dealuminated HY zeolite: a combined solid-state NMR and theoretical calculation study. J Am Chem Soc 2007;129(36):11161–71.
[58] Mayandi J, Marikkannan M, Ragavendran V, Jayabal P. Hydrothermally synthesized Sb and Zn doped SnO2 nanoparticles. J Nanosci Nanotechnol 2014;2:707–10.
[59] Elmadani AA, Radović I, Tomić NZ, Petrović M, Stojanović DB, Heinemann RJ, et al. Hybrid denture acrylic composites with nanozirconia and electrospun polystyrene fibers. PLoS One 2019;14(12).
[60] Zhan S, Li D, Liang S, Chen X, Li X. A novel flexible room temperature ethanol gas sensor based on SnO2 doped poly-diallyldimethylammonium chloride. Sensors 2013;13(4):4378–89.
[61] Dzwigaj S, Janas J, Gurgul J, Socha RP, Shishido T, Che M. Do Cu (II) ions need Al atoms in their environment to make CuSiBEA active in the SCR of NO by ethanol or propane? A spectroscopy and catalysis study. Appl Catal B 2009;85(3–4):131–8.
[62] Song S, Di L, Wu G, Dai W, Guan N, Li L. Meso-Zr-Al-beta zeolite as a robust catalyst for cascade reactions in biomass valorization. Appl Catal B 2017;205:393–403.
[63] Rauta PR, Manivasakan P, Rajendran V, Sahu BB, Panda BK, Mohapatra P. Phase transformation of ZrO2 nanoparticles produced from zircon. Phase Transit 2012;85(1–2):13–26.

[64] Li J, Chen C, Li J, Li S, Dong C. Synthesis of tin-glycerate and it conversion into SnO2 spheres for highly sensitive low-ppm-level acetone detection. J Mater Sci Mater Electron 2020;31(19):16539–47.
[65] Selli E, Forni L. Comparison between the Surface Acidity of Solid Catalysts Determined by TPD and FTIR Analysis of Pre-Adsorbed Pyridine. Micropor Mesopor Mater 1999;31(1–2):129–40.
[66] Szuber J, Czempik G, Larciprete R, Koziej D, Adamowicz B. XPS study of the L-CVD deposited SnO2 thin films exposed to oxygen and hydrogen. Thin Solid Films 2001; 391(2):198–203.
[67] Larciprete R, Borsella E, De Padova P, Perfetti P, Faglia G, Sberveglieri G. Investigations of radiation photoemission analysis of ArF lase deposited tin oxide. Thin Solid Films 1998;323:291–5.
[68] Crist B. V. Handbook of monochromatic XPS spectra. Vol.2: Commercially pure binary oxides. Mountain View (CA): XPS International LLC 1999.
[69] Song M, Wu Y, Zhao Y, Du C, Su Y. Structural insight on defect-rich tin oxide for smart band alignment engineering and tunable visible-light-driven hydrogen evolution. Inorg Chem 2020;59(5):3181–92.
[70] A.A. Korkmaz L.O. Ahmed R.O. Kareem H. Kebiroglu T. Ates N. Bulut et al. Theoretical and experimental characterization of Sn-based hydroxyapatites doped with Bi J Aust Ceram Soc 58 3 2022 803 815.
[71] Inshyna OI, Prudius SV, Brei VV. Superacid L-Sites on the Surface of Ternary ZrO2-SiO2-Al2O3 and ZrO2-SiO2-SnO2 Oxides. Theor Exp Chem 2022;58(4):269–75.
[72] Tang B, Dai W, Wu G, Guan N, Li L, Hunger M. Improved postsynthesis strategy to Sn-Beta zeolites as Lewis acid catalysts for the ring-opening hydration of epoxides. ACS Catal 2014;4(8):2801–10.
[73] Dementjev AP, Ivanova OP, Vasilyev LA, Naumkin AV, Nemirovsky DM, Shalaev DY. Altered layer as sensitive initial chemical state indicator. J Vac Sci Technol A 1994;12(2):423–7.
[74] García A, Monti E, Ventimiglia A, Dimitratos N, Miguel PJ, López ML, et al. Zr supported on non-acidic sepiolite for the efficient one-pot transformation of furfural into γ-valerolactone. Biomass Bioenergy 2023;170.
[75] Oliviero L, Vimont A, Lavalley J-C, Romero Sarria F, Gaillard M, Maugé F. 2,6-Dimethylpyridine as a probe of the strength of Brønsted acid sites: study on zeolites. Application to alumina. PCCP 2005;7(8):1861–9.
[76] Ren X, Zhang Z, Wang Y, Lu J, An J, Zhang J, et al. Capping experiments reveal multiple surface active sites in CeO2 and their cooperative catalysis. RSC Adv 2019;9(27):15229–37.
[77] Shao Y, Li Q, Dong X, Wang J, Sun K, Zhang L, et al. Cooperation between hydrogenation and acidic sites in Cu-based catalyst for selective conversion of furfural to γ-valerolactone. Fuel 2021;293.
[78] He J, Li H, Xu Y, Yang S. Dual acidic mesoporous KIT silicates enable one-pot production of γ-valerolactone from biomass derivatives via cascade reactions. Renew Energ 2020;146:359–70.
[79] Gao X, Yu X, Peng L, He L, Zhang J. Magnetic Fe3O4 nanoparticles and ZrO2-doped mesoporous MCM-41 as a monolithic multifunctional catalyst for γ-valerolactone production directly from furfural. Fuel 2021;300.
[80] Wang T, He J, Zhang Y. Production of γ-valerolactone from one-pot transformation of biomass-derived carbohydrates over chitosan-supported ruthenium catalyst combined with zeolite ZSM-5. Eur J Org Chem 2020;2020(11):1611–9.
[81] Tan J, Liu Y, Li M, Li Hu, Yang S. One-step catalytic upgrading of bio-based furfural to γ-valerolactone actuated by coordination organophosphate–Hf polymers. Sustain Energy Fuels 2022;6(2):484–501.